Pertanika J. Sci. & Technol. 33 (3): 1273 - 1299 (2025)

PERTANIKA JOURNALS

SCIENCE & TECHNOLOGY

Journal homepage: http://www.pertanika.upm.edu.my/

Development of a Two-board Potentiostat for Square Wave Anodic Stripping Voltammetry: Prospects for Heavy Metal Monitoring

Siti Nur Hanisah Umar[1]*, Elmi Abu Bakar[2], Mohammad Nishat Akhtar[2], Noorfazreena Mohammad Kamaruddin[2] and Naoki Uchiyama[3]

[1]School of Mechanical Engineering, Engineering Campus, Universiti Sains Malaysia, Nibong Tebal, 14300, Malaysia

[2]School of Aerospace Engineering, Engineering Campus, Universiti Sains Malaysia, Nibong Tebal, 14300, Malaysia

[3]Department of Mechanical Engineering, Toyohashi University of Technology, Tenpaku Cho, Hibarigaoka, Toyohashi-shi, Aichi, Japan

ABSTRACT

Heavy metals such as cadmium, lead, arsenic, mercury, and chromium are harmful to human health, even in a trace amount. Despite existing guidelines and regulations for handling these toxic substances, mortality cases among wild animals due to heavy metal poisoning continue to occur. To effectively investigate the sources of heavy metal contaminants in the environment, it is essential to establish real-time monitoring systems across affected areas. This paper presents the design and development of a potentiostat device (HMstat) with the capability to perform a square wave anodic stripping voltammetry (SWASV). The HMstat was realized using a two-board type potentiostat design, incorporating through-hole technology for the analog component and the myRIO platform for the digital component. Performance evaluations indicated that the HMstat is capable of performing the SWASV method. The results demonstrated that the HMstat achieved an accuracy of 99.014%, remained within the tolerance range of components used and surpassed the existing solution.

Keywords: Heavy metal, potentiostat, square wave anodic stripping voltammetry

ARTICLE INFO

Article history:
Received: 31 August 2024
Accepted: 16 January 2025
Published: 26 March 2025

DOI: https://doi.org/10.47836/pjst.33.3.09

E-mail addresses:
snhanisah@usm.my (Siti Nur Hanisah Umar)
meelmi@usm.my (Elmi Abu Bakar)
nishat@usm.my (Mohammad Nishat Akhtar)
fazreena@usm.my (Noorfazreena Mohammad Kamaruddin)
uchiyama@tut.jp (Naoki Uchiyama)
*Corresponding author

INTRODUCTION

Heavy metals such as cadmium, lead, arsenic, mercury, and chromium are toxic even in small amounts. They pose significant risks to human health and the environment

e-ISSN: 2231-8526

due to their toxicity and ability to accumulate in living organisms. Environmental contamination by heavy metals is predominantly due to anthropogenic activities. These metals possess specific properties that make them suitable for various industrial applications, including metal finishing, electrical and electronics, textiles, food processing, chemicals, palm oil, rubber, wood, and iron and steel manufacturing (IARC, 2012).

Despite increased awareness and regulations surrounding the use of heavy metals in Malaysia, cases of heavy metal poisoning continue to occur. For instance, in recent cases in Sabah, Malaysia, three Borneo pygmy elephants were reported to have died from heavy metal poisoning, with high levels of cadmium found in their livers and kidneys. However, the source of the heavy metal remains unknown (Vanar, 2021). To effectively investigate the sources of heavy metal contaminants in the environment, it is essential to establish real-time monitoring programs that evaluate water quality and agricultural practices across affected areas, highlighting the need for on-site monitoring techniques.

Traditionally, spectrometric techniques have been used to detect heavy metals in the environment. Various instruments have been developed for this purpose, including spectrometric techniques such as inductively coupled plasma mass spectrometry (ICP-MS), inductively coupled plasma atomic emission spectrometry (ICP-AES), inductively coupled plasma-optical emission spectrometry (ICP-OES), flame atomic absorption spectrometry (F-AAS), and graphite furnace atomic absorption spectrometry (GF-AAS). These instruments are highly sensitive and selective and have been used to detect cadmium levels in water (Ahmed et al., 2020; Zanuri et al., 2020), air (Azid et al., 2018; Mohamed et al., 2014), soil (Chaudhary et al., 2020; Kusin et al., 2018), fish (Ishak et al., 2020; Poong et al., 2020), tobacco (Janaydeh et al., 2019), and human blood (Zulkifli et al., 2019).

However, these spectrometric instruments are expensive, have complex operational procedures, and require skilled and trained personnel. Additionally, these instruments are laboratory-based, bulky, and unsuitable for in-situ application, making samples susceptible to contamination during storage and transportation from site to laboratory, potentially leading to inaccurate results (Fakude et al., 2020; Lu et al., 2018). To avoid contamination, the in-situ monitoring of heavy metals is necessary. Electrochemical techniques are well-suited for in-situ monitoring due to their rapid analysis, ease of use, and adaptability for integration into compact circuits, making them ideal for portable and in-situ applications (Bansod et al., 2017; Lu et al., 2018; Lv et al., 2017).

The commercial electrochemical instruments, which the potentiostats can be purchased as bench-top instruments that offer a broad operating potential range, user-friendly software for data interface and display, and a wide range of specialized applications, including characterization of batteries, fuel cells, biosensors, corrosion, environmental monitoring, and the electrochemical synthesis of materials (Irving et al., 2021). However, in practice, only a few of the built-in features are frequently used. This often makes

commercial potentiostats overly complex and overpriced, particularly when only simple electroanalytical applications are required (Tichter et al., 2023). Additionally, the bulky size of bench-top potentiostats limits their application in laboratory environments.

In contrast, hand-held potentiostats, such as the EmStat4S from PalmSens and the DropStat from Metrohm, offer portability, making them suitable for in-situ applications. However, commercial potentiostats are typically distributed as “black boxes," making it impossible to reprogram and modify the devices (often for warranty reasons) to accommodate measurement routines beyond the standard functions (Dryden & Wheeler, 2015; Tichter et al., 2023).

Nowadays, several designs of self-built potentiostat have been reported for heavy metal ion detection (Adams et al., 2019; Cordova-Huaman et al., 2021; Nemiroski et al., 2014; Rowe et al., 2011; Umar et al., 2021; Umar, Bakar et al., 2020; Umar, Akhtar et al., 2020; Wu et al., 2017). Most designs implement a single board type with surface-mounted integrated circuits, which can be manufactured in small sizes regardless of the component complexity. These designs typically feature 12-bit or higher input/output resolution, sufficient for performing square wave anodic stripping voltammetry method (SWASV), a widely used technique for rapid analysis of heavy metals ions (Bansod et al., 2017; Borrill et al., 2019). However, they require skilled personnel and sophisticated tools for fabrication and component assembly, creating hindrances for researchers who wish to undertake in-house fabrication and modification.

An alternative approach is the two-board type potentiostat, where the digital (signal controller) and the analog components are designed on separate boards (Li et al., 2018; Meloni, 2016; Umar et al., 2018). This type of potentiostat implements an off-the-shelf board as the digital component and a custom-fabricated daughterboard with through-hole technology for the analog component. This design allows in-house self-fabrication and modification, regardless of the researcher's background, even with limited fabrication skills and equipment. One of the self-built potentiostat developments is an Arduino-based potentiostat fabricated using simple through-hole electronic components capable of performing simple electrochemical experiments. However, the Arduino-based potentiostat requires external Analog-to-Digital Converter (ADC) and Digital-to-Analog Converter (DAC) components, making the design more complicated. Moreover, the Arduino-based potentiostat has limitations in operating high-frequency electrochemical methods such as SWASV (Li et al., 2018; Meloni, 2016; Umar et al., 2018).

Thus, the main aim of this study is to design and develop a potentiostat device (HMstat) capable of performing SWASV. This study provides a detailed description of the development of the HMstat and evaluates its ability to execute the SWASV method using cell replication. The testing is limited to imitation scenarios. Although it does not involve real heavy metal samples, the HMstat is intended for future applications in heavy metal detection.

METHODOLOGY

Design of HMstat

The proposed device, HMstat, is designed using a two-board approach. The design comprises three components (Figure 1): the analog component, known as the potentiostat read-out circuit component (PRCC); the digital component, referred to as the control signal component (CSC); and the graphical user interface (GUI).

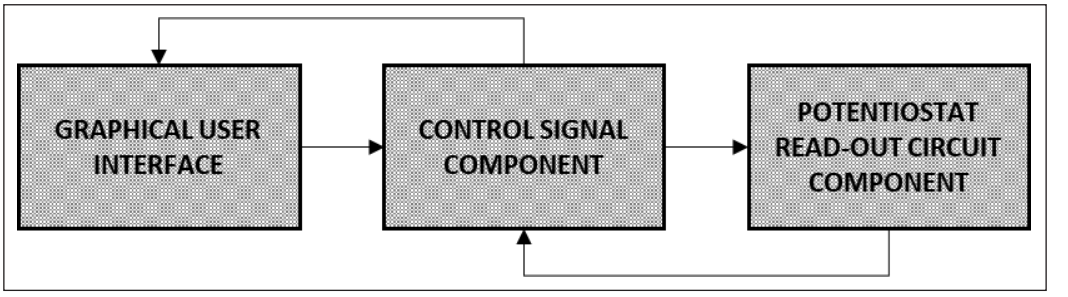

Figure 1. General overview of components of HMstat

Potentiostat Read-out Circuit Component PRCC

The PRCC is designed by implementing through-hole technology. This technology facilitates the fabrication and modification process of the PRCC regardless of researchers' backgrounds, even with limited skills and tools. The PRCC comprises two primary components: the potential control part (PCP) and the current measurement part (CMP).

Potential Control Part

The PCP's role is to regulate the interfacial potential at the working electrode (WE) concerning the reference electrode (RE) through the counter electrode (CE) in the electrochemical cell. The PCP is structured into two stages, utilizing distinct operational amplifier configurations, as illustrated in Figure 2. The first stage is the summing amplifier (OA_{SUM}), and the second is the voltage follower (OA_{FOL}), which is positioned in the negative feedback loop of OA_{SUM}. OA_{FOL} functions to limit any potential current flow through the RE and serves as a unity gain buffer. The potential at the WE is controlled by applying a voltage signal, V_{ap}, to the negative input of OA_{SUM}. As V_{ap} deviates from the fixed potential of RE, the output of OA_{SUM} adjusts to direct current flow between the CE and WE, thereby equalizing the positive and negative inputs of OA_{SUM}.

Current Measurement Part

The second component of PRCC is the CMP, which consists of a single-stage trans-impedance amplifier (OA_{TIA}), as depicted in Figure 2. The purpose of the CMP is to measure

the current passing through the electrochemical cell between the CE and WE, which corresponds to the varying potential output from OA_{SUM}. This current is quantified as a voltage drop across the feedback resistor (R_{gain}) of OA_{TIA}. The output of OA_{TIA} is further amplified before being recorded.

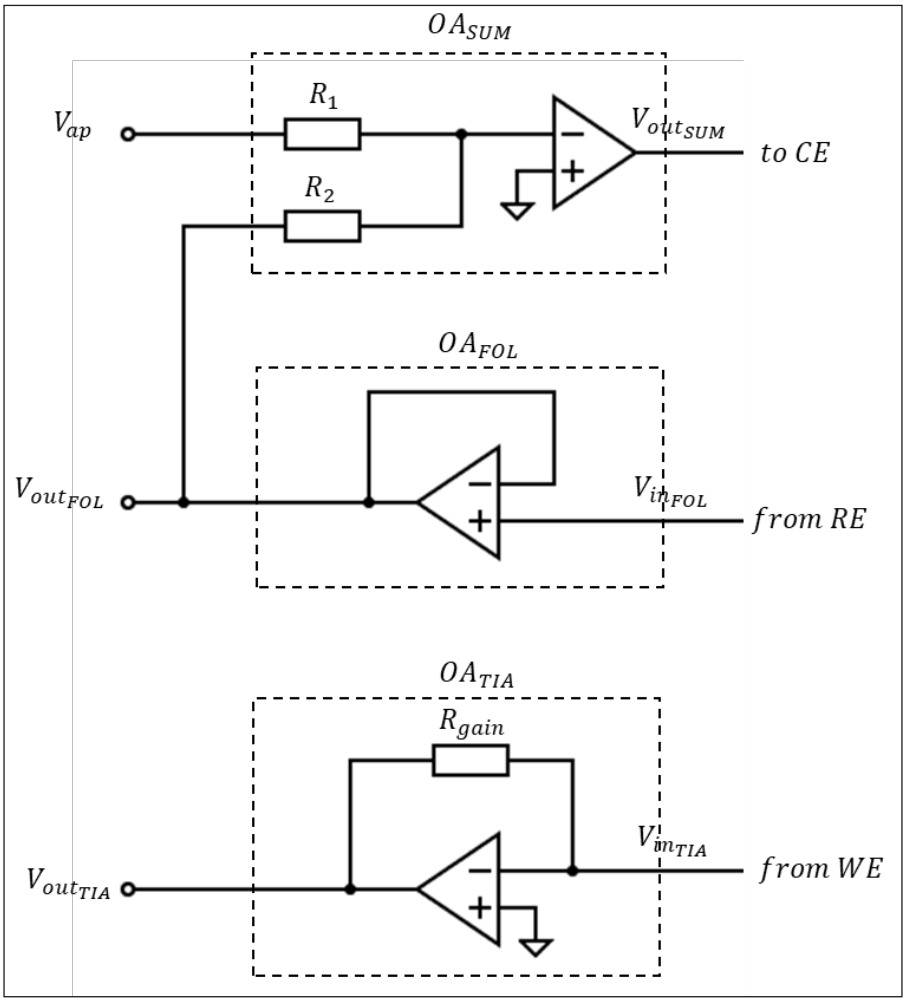

Figure 2. Block diagram of potential control part and current measurement part in potentiostat read-out circuit component

Control Signal Component

The CSC for HMstat was developed using the myRIO platform as the digital core. Under this platform, the signal generation/acquisition and dedicated Graphical User Interface (GUI) was developed to allow for real-time signal monitoring. Several attributes of the myRIO platform render it well-suited to serve as the CSC for HMstat. Notably, it

comes equipped with a built-in 12-bit DAC and ADC, offering analog output and input functionality that can be effectively utilized in both polar directions. This capability is accessible through the miniSystem port (MSP C) (Figure 3), which includes:

- Power Outputs: +5 V, +15 V, and -15 V power outputs.
- Analog Input Channels: Two differential analog input channels (AI0+/AI0- and AI1+/AI1-). It can be used to measure signals up to ±10 V.
- Analog Output Channels: Two single-ended analog output channels (AO0 and AO1). It can be used to generate signals up to ±10 V.
- General-Purpose Digital Lines: Eight general-purpose digital lines, capable of 3.3 V output and 3.3 V or 5 V compatible input (DIO0 to DIO7).
- Reference Grounds: DGND serves as a reference for digital lines and +5 V power output, while AGND serves as a reference for analog input and output, as well as +15V and -15V power outputs.

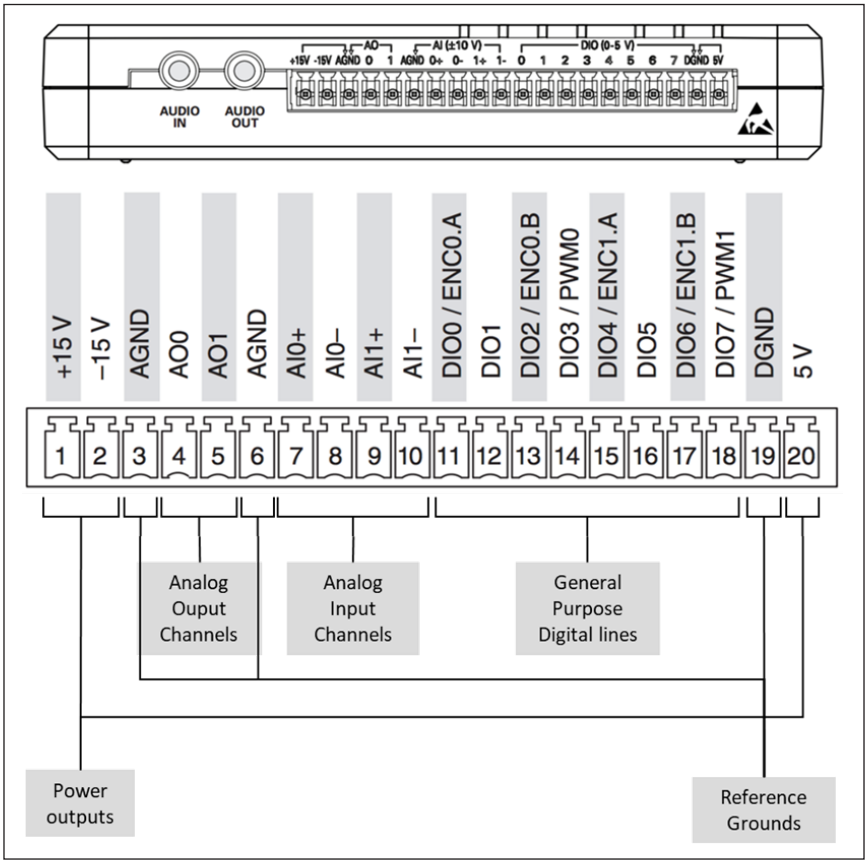

Figure 3. Input-output of CSC

Signal Generation and Process

Signal generation, acquisition, and processing are designed and executed within the CSC using the LABVIEW graphical programming environment. Figure 4 depicts the basic structure of the LABVIEW program. It comprises six main components: loops, signal blocks, an analog output block, an analog input block, data collection blocks, a measurement file block, and waveform charts blocks.

The loops used include the while loop, case structure loop, for loop, and control loop. The analog output block writes the value or passes the generated signal to the analog output channel of AO0 (analog output 0). The analog input block reads value or acquires signal from the two analog input channels, AI0 and AI1 (analog input 0 and analog input 1). The data collection blocks collect signals at each time step of the signal writes (generates) and reads (acquires) and return them as collected signal values along with time data. The measurement file block stores the data collected by the data collection block and stores it in Microsoft Excel files (.xlsx). The waveform chart blocks display the generated and acquired signal, enabling real-time monitoring by the user.

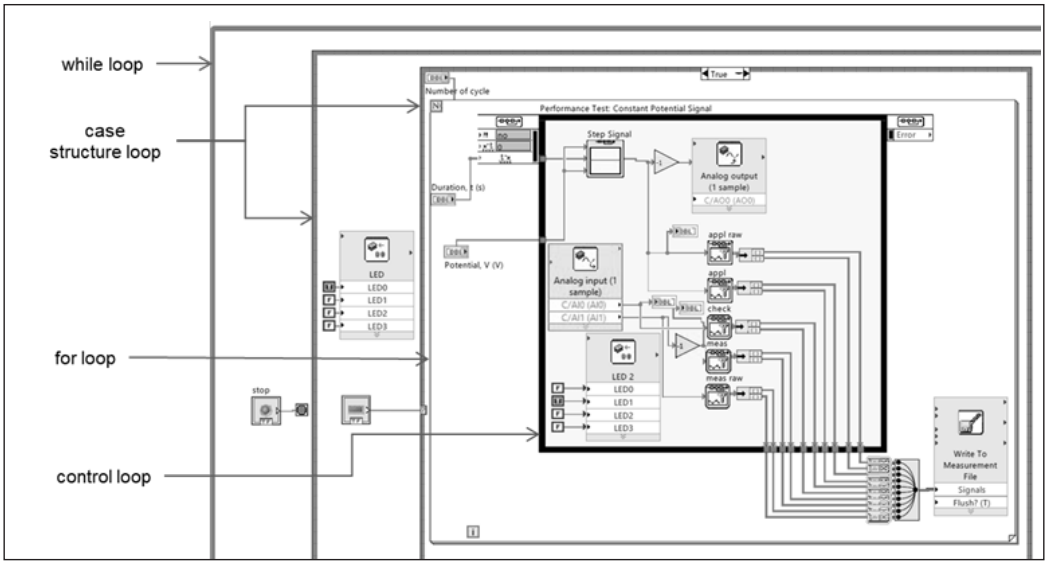

Figure 4. LABVIEW graphical program

The signal block is used to generate the desired potential signals. For HMstat to perform the SWASV method, three signals are designed: constant, ramp, and square wave voltammetry (SWV). These three signals are the core elements used in the SWASV method. Constant and SWV signals are the core elements used in the SWASV method, while the ramp signal is a constituent of cyclic voltammetry (CV), performed prior to measurement as a surface treatment for the electrode, particularly the screen-printed electrode. This process

aims to achieve a proper baseline and a stable response during heavy metal detection or measurement (Bernalte et al., 2020).

Generation of Constant Signal

The basic parameters for generating the constant signal are the desired constant potential and the duration of the applied constant potential. The constant signal is generated using a step signal block (Figure 5). This block requires three input parameters: the initial, final, and step time. The initial and the final values are set to the desired constant potential, and the step time determines the duration for which the constant potential is applied.

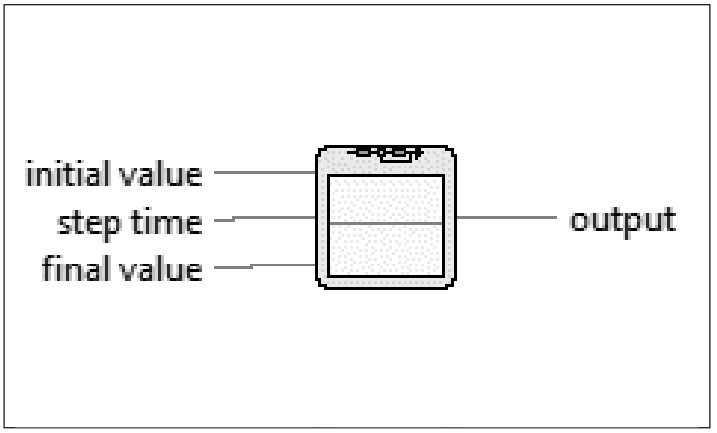

Figure 5. Step signal block

Generation of the Ramp Signal

The key parameters for generating the ramp signal are the initial and final potential, along with the scan rate. The ramp signal is generated using a ramp signal block (Figure 6), which requires three input parameters: the initial output, the start time, and the slope of the ramp signal. The initial output corresponds to the initial potential of the ramp signal, the start time is set to 0 for all measurements, and the slope is determined by the scan rate.

Generation of SWV Signal

SWV signal combines a square wave and staircase signal. The main parameters in SWV are the initial and final potential, the modulation amplitude, the step amplitude, and the frequency of the SWV signal. The SWV signal is generated using a combination of the ramp signal block (Figure 6), the discrete signal block [Figure 7(a)], and the pulse signal block [Figure 7(b)]. The ramp signal block is first discretized using the discrete signal block to form a staircase signal, which is then superimposed with the square wave signal generated

using the pulse signal block. The input parameters for the ramp signal block include the initial potential as the initial output, the start time of 0, and the slope as a product of the step amplitude and the frequency of the SWV signal.

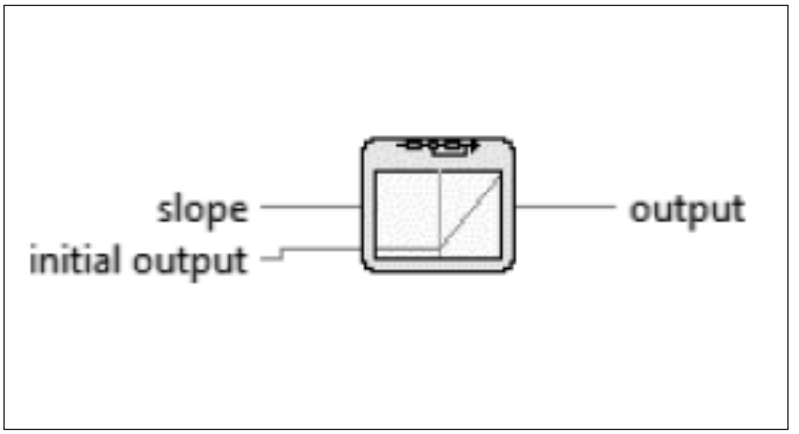

Figure 6. Ramp signal block

The input parameters for the discrete signal block are the sample period and the sample skew. The sample period is set as 1/frequency of the SWV signal, and the skew is set to 0. The pulse signal block requires five input parameters: the start time, amplitude, offset, duty cycle, and period. The start time is set to 0, the amplitude is half of the modulation amplitude, the offset is negative half of the modulation amplitude, the duty cycle is 50%, and the period is 1/frequency.

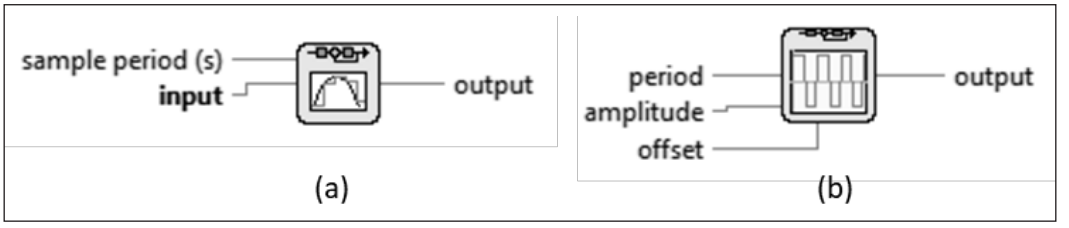

Figure 7. Discrete signal block and pulse signal block

User Interface

A graphic user interface (GUI) allows the user to control the test parameters and provides real-time monitoring for both signal generation and acquisition. The GUI is designed and developed using the LABVIEW program. The three basic signals, constant, ramp and SWV, are integrated into the GUI under the 'Cell Replication Bench Test' tab (Figure 8).

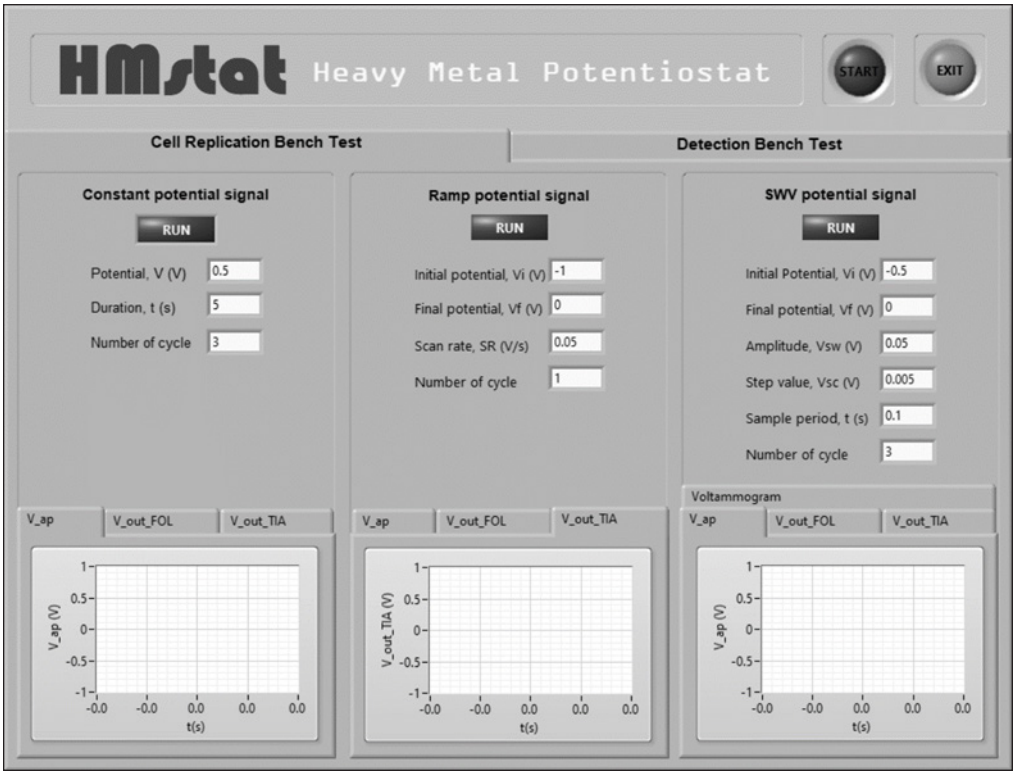

Figure 8. Graphical user interface developed for real-time performance monitoring

Fabrication of HMstat

This section describes the electronic components used to fabricate and assemble the HMstat's PRCC. Table 1 lists all required electronic components for building the PRCC. Initially, the electronic components were assembled on a breadboard to assess their functionality. Once confirmed, they were permanently soldered onto a stripboard.

A single-sided stripboard is used, as shown in Figure 9. The size of the stripboard is 13 × 16 [Figure 10(a)]. The stripboard is cut into the desired size using a circuit board cutter. The thin copper lanes are broken at the appropriate locations using a drill bit. The locations of the broken copper lanes are shown in Figure 10(b). The placement of electronic components, such as the operational amplifier (LM324N), resistors (R1 and R2), and terminal blocks (2-PMSTB and 3-PMSTB1,2,3), is illustrated in Figure 10(c). The placement of wires is shown in Figure 10(d). The feedback resistor, R_{gain}, is connected to PRCC through a 2-pin male screw terminal block (2-PMSTB) to allow for flexibility in operating the current range [Figure 10(e)]. The R_{gain} value can be replaced with a larger or smaller resistance value for a smaller or larger current range.

Table 1
Bill of materials (1 MYR = 0.2127 EUR = 0.2218 USD)

Designator	**Component**	**Unit**	**Cost per unit -currency**	**Total cost - currency**	**Source of materials**	**Material type**
R_1,R_2	Resistor 10kΩ	2	0.5 MYR	1.0 MYR	Shopee	Metal
R_{gain}	Resistor 499kΩ	1	0.5 MY	0.5 MYR	Shopee	Metal
$R_{WE/RE}$	Resistor 100kΩ	1	0.5 MYR	0.5 MYR	Shopee	Metal
LM324N	IC Quad Op-Amp LM324N	1	2.0 MYR	2.0 MYR	Shopee	Other
LM324N	IC Quad Op-Amp LM324 socket	1	0.4 MYR	0.4 MYR	Shopee	Other
Wire	Jumper wire	20	0.2 MYR	4.0 MYR	Shopee	Metal/ Polymer
Stripboard	Single-sided stripboard	1	2.0 MYR	2.0 MYR	Shopee	Other
3-PMSTB	3-pin Male Screw terminal block	3	1.0 MYR	3.0 MYR	Shopee	Other
2-PMSTB	2-pin Male Screw terminal block	1	1.0 MYR	1.0 MYR	Shopee	Other
CSC	myRIO	1	3984.0 MYR	3984.0 MYR	Element14	Other
Cell replication	Prototype breadboard	1	25.0 MYR	25.0 MYR	Element14	Other

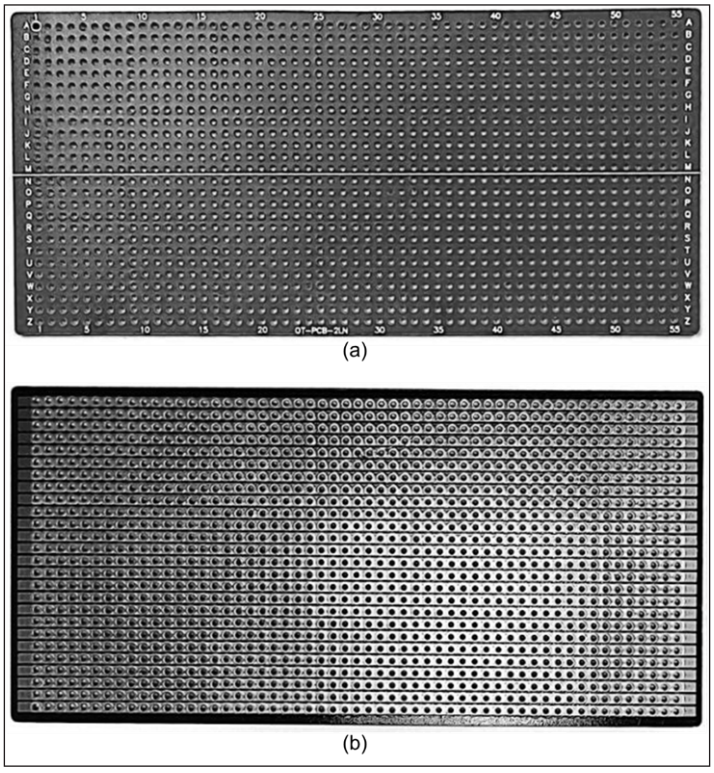

Figure 9. (a) Stripboard front (no copper strip) and (b) stripboard rear (with copper strip)

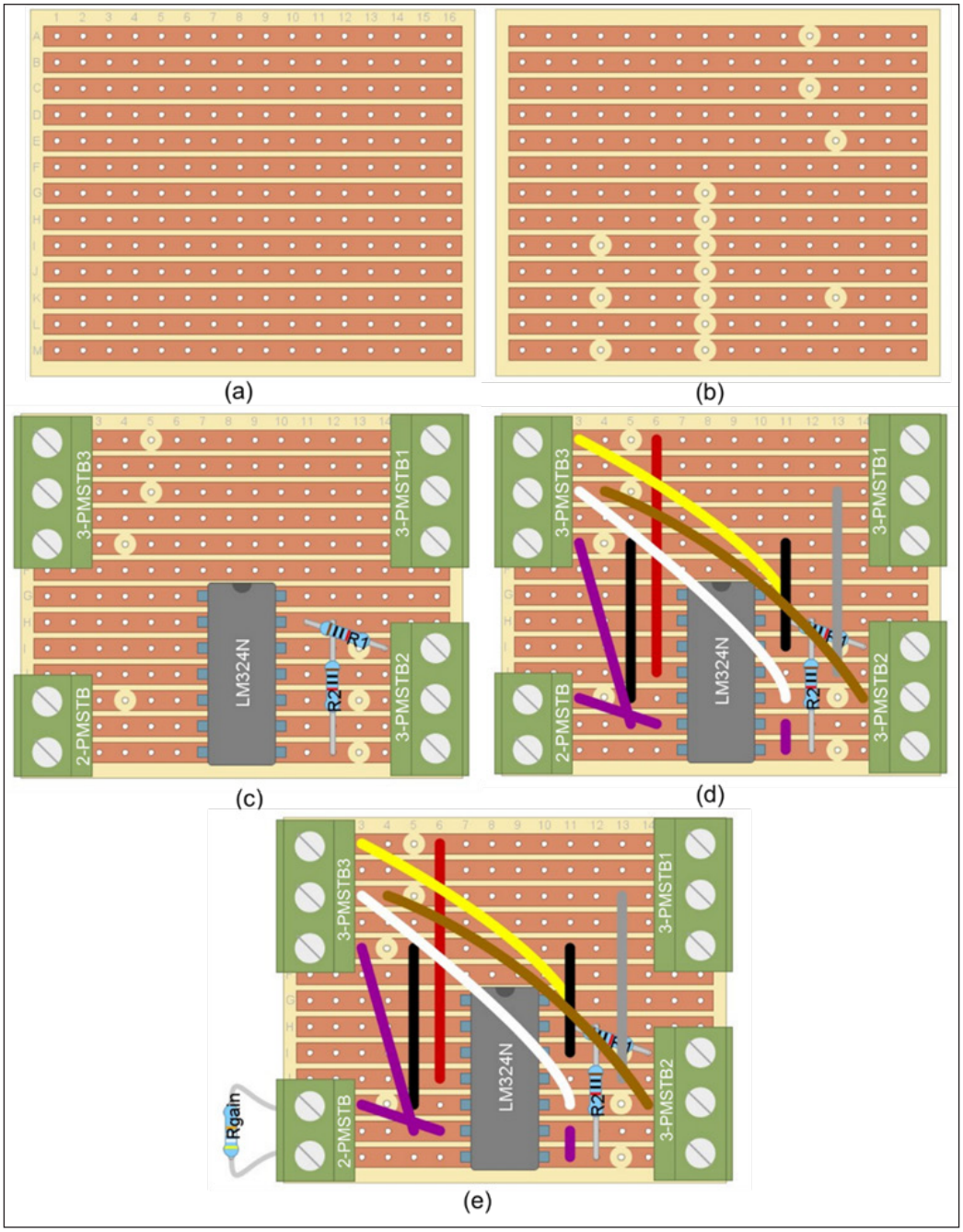

Figure 10. (a) Stripboard cutout dimension of 16 × 13 (front). (b) Breakage points (rear). (c) Placement of electronic component on stripboard (LM324N, R1 and R2, 3-PMSTB1,2,3, and 2-PMSTB2). (d) Placement of wires. (e) Placement of R_{gain}

The connection between the PRCC and CSC is illustrated in Figure 11. Six interconnections between CSC and PRCC are involved. The CSC provides dual-polarity power outputs of +15V and -15V to the LM324N operational amplifier, with AGND serving as the reference point for these power outputs. Additionally, the voltage signal, denoted as V_{ap}, generated by the CSC, is transmitted to the PRCC via the analog output (AO0). The CSC, in turn, receives two distinct signals from the PRCC through two differential analog inputs (AI0+ and AI1+). The signals obtained from AI0+ and AI1+ correspond to the output signals from the OA_{FOL}, $V_{out_{FOL}}$ and, OA_{TIA}, $V_{out_{TIA}}$ of the PRCC, respectively. A summary of the connections is provided in Table 2.

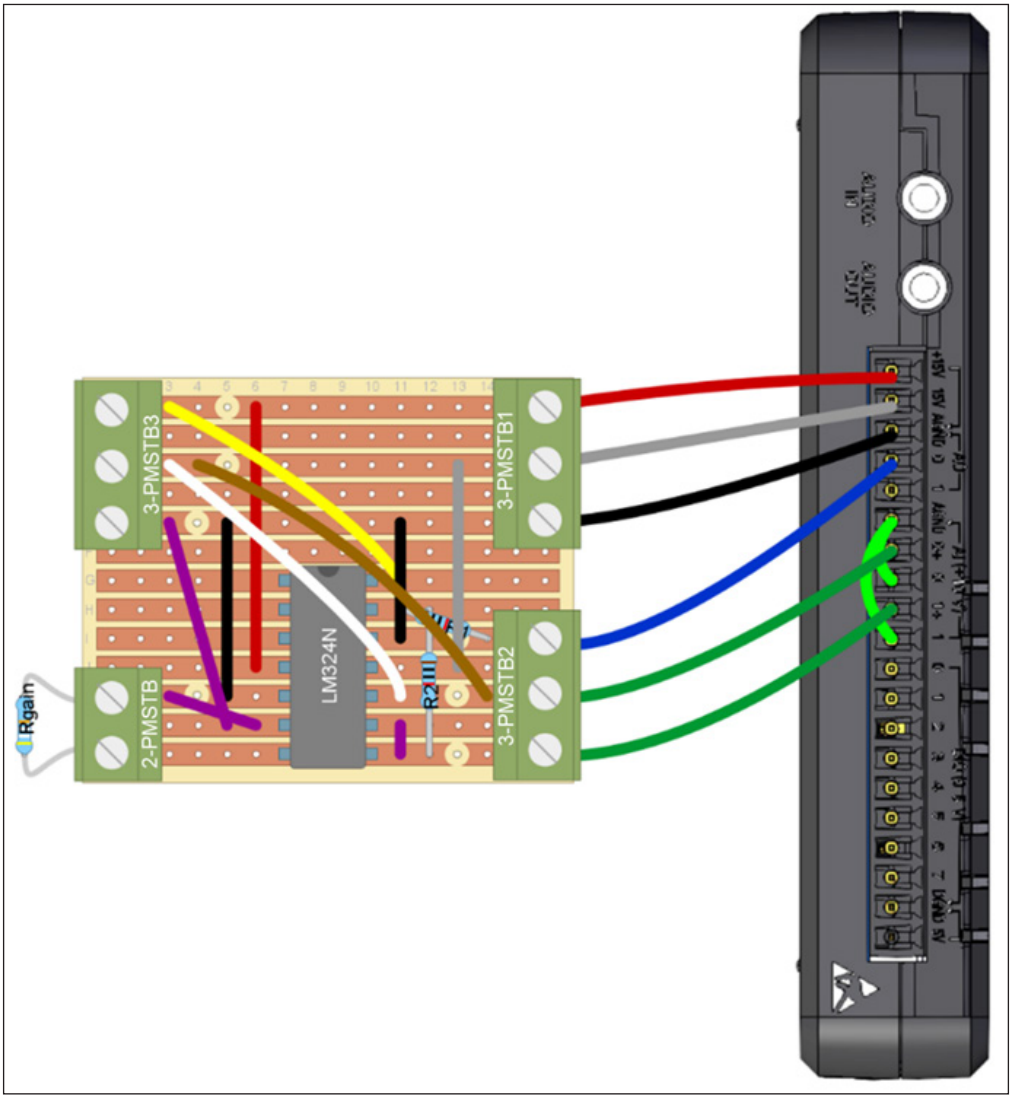

Figure 11. Connection of PRCC to CSC

Table 2
Summary connection between CSC and PRCC

PRCC			CSC		Wire colour
Description	**Symbol**	**Terminal block**	**Description**	**Symbol**	
Positive supply of LM324N operational amplifier	+V	3-PMSTB1_1	Positive power output	+15V	—
Negative supply of LM324N operational amplifier	-V	3-PMSTB1_2	Negative power output	-15V	—
Inverting input of summing amplifier (LM324N 4)	$V_{in_{SUM}}$	3-PMSTB2_1	Analog output 0	AO0	—
Output of voltage follower (LM324N 3)	$V_{out_{FOL}}$	3-PMSTB2_2	Analog input	AI0+	—
Output of transimpedance amplifier (LM324N 3)	$V_{out_{TIA}}$	3-PMSTB2_3	Analog input	AI1+	—
Positive input of summing amplifier (LM324N 2)	-	3-PMSTB1_3	Ground	AGND	—
The positive input of transimpedance amplifier (LM324N 3)	-	3-PMSTB1_3	Ground	AGND	—

RESULTS AND DISCUSSION

This section describes the assessment of the HMstat in terms of device functionality and accuracy. The performance of the HMstat is evaluated using a cell replication bench test. This test employs a single resistance between RE ($V_{in_{FOL}}$) and WE ($V_{in_{TIA}}$), representing the primary electrochemical cell. This test uses a resistance value ($R_{RE/WE}$) of 100 kΩ ± 5%.

Device Functionality

The HMstat is first linked to the cell replication of $R_{RE/WE}$, as illustrated in Figure 12. To interface the cell replication with the HMstat, the output of OA_{SUM} and the positive input of OA_{FOL} are connected to one terminal of $R_{RE/WE}$, while the other terminal of $R_{RE/WE}$ $R_{RE/WE}$ is connected to the negative input of OA_{TIA} [Figure 12(a)]. As illustrated in the circuit layout [Figure 12(b)] and the prototype [Figure 12(c)], the 3-pin male screw terminal block 3 (3-PMSTB3) served as the interconnection between cell replication and the HMstat.

The HMstat is powered using an external power supply cable and connected to the personal computer via a USB cable. The real-time monitoring GUI is launched (Figure 8). Pressing the green start button activates the GUI, as indicated by the illumination of LED0 on the myRIO platform. Under the "Cell Replication Bench Test" tab, the parameters of the signal testing are set.

For constant V_{ap} signal, 11 different constant signals (-0.5V, -0.4V, -0.3 V, -0.2 V, 0V, 0.1 V, 0.2 V, 0.3 V, 0.4 V, and 0.5 V) are applied for a duration of 20 seconds. The ramp

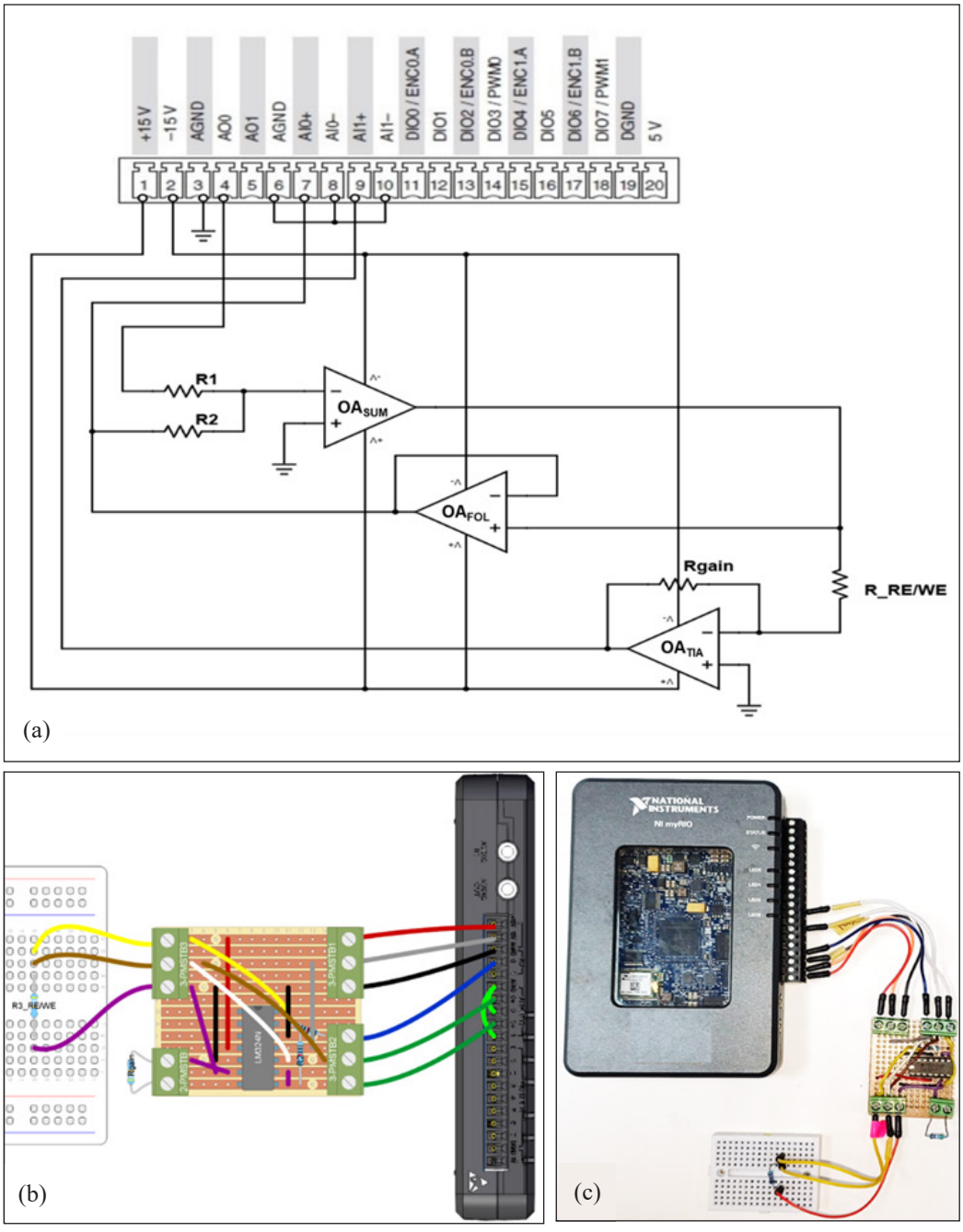

Figure 12. (a) The circuit diagram, (b) circuit layout, and (c) prototype of HMstat connected to cell replication

V_{ap} signal sweeps from an initial potential of -0.5 V to +0.5 V with a scan rate of 0.05 V/s. The SWV V_{ap} signal is scanned from an initial potential of -0.5 V to 0 V, with a modulation amplitude of 0.05 V, a step amplitude of 0.005 V, and a frequency of 10 Hz. Each signal is applied for a single cycle.

The measurement starts when the Run button is clicked. During the measurement, real-time signal generation and acquisition were monitored on the graph panel, as illustrated in Figure 13. The measurement can be stopped at any time by pressing the EXIT button. Upon completion, the stored data is available in .xlsx format for further manipulation and analysis.

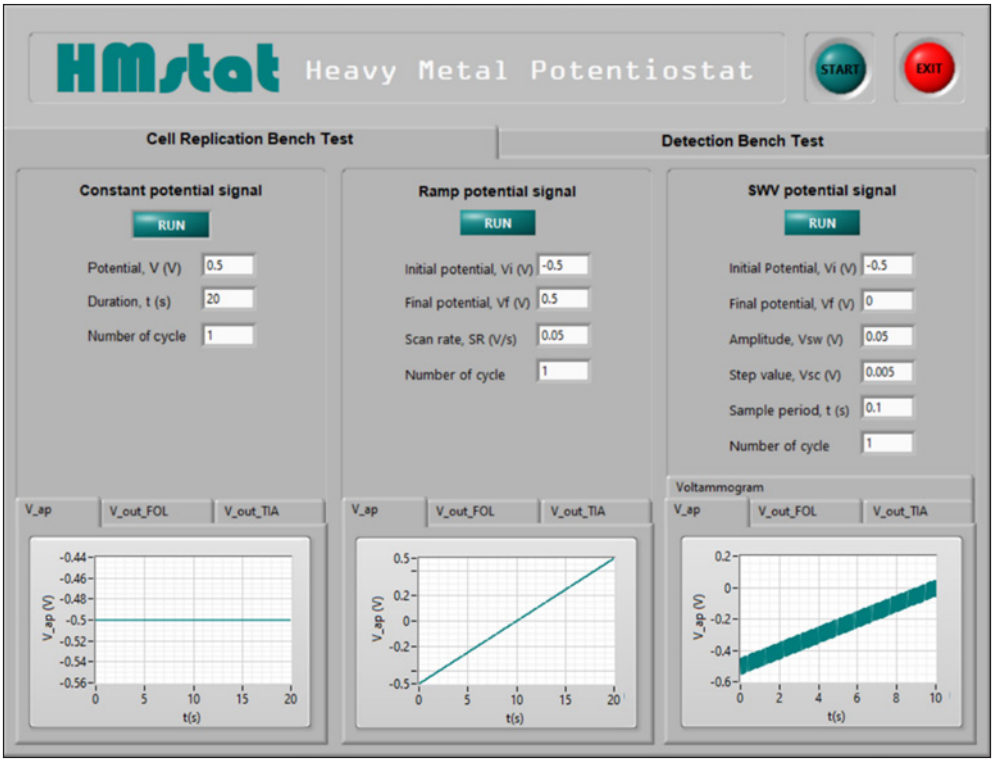

Figure 13. Real-time monitoring of signal generation and acquisition

The response of the HMstat is obtained through the output of PCP and CMP. The output results of PCP are acquired as $V_{out_{FOL}}$ from the PRCC, accessed through AI0+ of the CSC. The output results of CMP are acquired as $V_{out_{TIA}}$ from the PRCC, accessed through AI1+ of the CSC. The formulation of the output from PCP and CMP is derived based on Kirchhoff's law and Ohm's law. Ideally, the current flow into the input terminal of the operational amplifier is zero. Thus, the measured voltage applied to the WE, $V_{out_{FOL}}$

is expressed in terms of the applied voltage signal, V_{ap}, as given in Equation 1. Given that $R_1 = R_2 = 10\ k\Omega$, the magnitude of $\mathrm{V_{out_{FOL}}}$ is expected to be equal to V_{ap}.

$$V_{out\ FOL} = -\frac{R_2}{R_1}V_{ap} \quad [1]$$

The output results of PCP under constant, ramp, and SWV V_{ap} signals are shown in Figures 14(a)-(c). In Figure 14(a), 11 constant V_{ap} signals ranging from -0.5 V to 0.5 V are applied to PCP. The results demonstrate that the magnitude of $\mathrm{V_{out_{FOL}}}$ signals is consistent with the magnitude of V_{ap} signals, aligned with Equation 1, as $R_1 = R_2$, thus $\mathrm{V_{out_{FOL}}} = V_{ap}$. In Figure 14(b), the result of the ramp V_{ap} signal sweeping from -0.5 V to 0.5 V is shown, with $\mathrm{V_{out_{FOL}}}$ increasing in accordance with V_{ap}. The results shown in Figure 14(c) demonstrate that the PCP is capable of operating under the SWV V_{ap}signal. However, slight deviations and fluctuations were observed were observed. The deviation was particularly evident in the responses to the constant V_{ap}signals, while noise was present in the results for both constant and ramp V_{ap} signals.

The ideal current measurement can be expressed as shown in Equation 2. The experimental current measurement of HMstat is obtained as a voltage drop across the feedback resistor, R_{gain} as $\mathrm{V_{out_{TIA}}}$. The formulation is shown in Equation 3. Combining Equations 2 and 3, the expression for V_{out_TIA} in terms of V_{ap} is given in Equation 4. Since $R_{gain} = 499\ k\Omega$ and $R_{RE/WE} = 100k\Omega$, thus, $V_{out\ TIA} = 4.99V_{ap}$.

$$I_{WE/RE} = \frac{V_{ap}}{R_{RE/WE}} \quad [2]$$

$$I_{WE/RE} = \frac{V_{out\ TIA}}{R_{gain}} \quad [3]$$

$$\frac{V_{ap}}{R_{RE/WE}} = \frac{V_{out\ TIA}}{R_{gain}} \quad [4]$$

In Figures 15(a) – (c), the output results of CMP under constants, ramp, and SWV V_{ap} signals are shown. Figure 15(a) demonstrates the response of CMP to 11 constant V_{ap} signals ranging from -0.5 V to 0.5 V. The results indicate that the $\mathrm{V_{out_{TIA}}}$ signals are approximately five times the V_{ap} signals, consistent with Equation 4 as $R_{gain} = 499\ k\Omega$ and $R_{RE/WE} = 100k\Omega$; thus, $V_{out\ TIA} = 4.99V_{ap}$. The response of CMP under ramp V_{ap} signals [Figure 15(b)] also aligns with Equation 4, with $\mathrm{V_{out_{TIA}}}$ signals increasing with V_{ap} signals. The CMP is also capable of operating under SWV V_{ap} signals, with results following the applied signal. Similar to the result observed for the PCP, deviations and noise were also present in each CMP result.

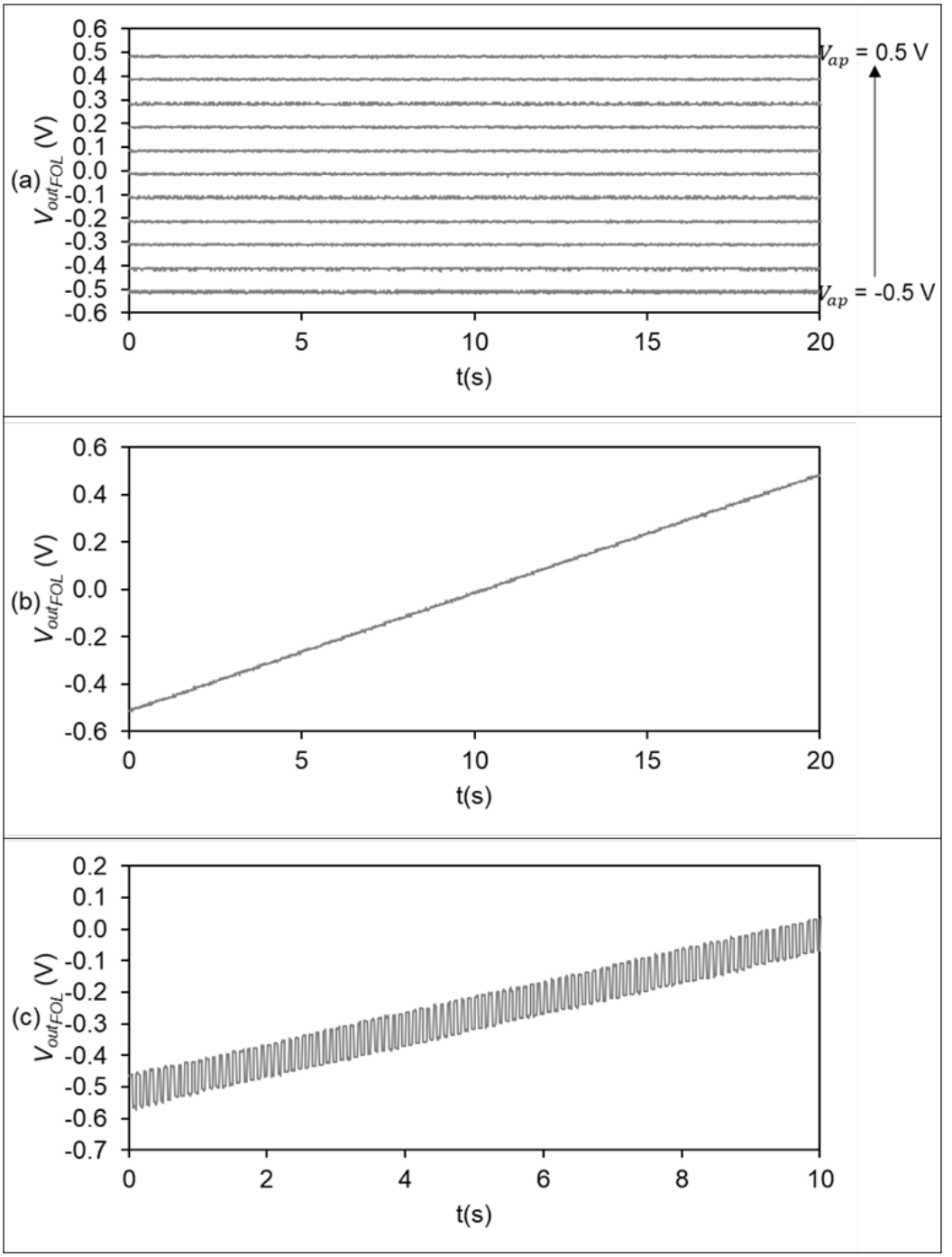

Figure 14. The output of PCP under (a) constant, (b) ramp, and (c) SWV V_{ap} signals, respectively

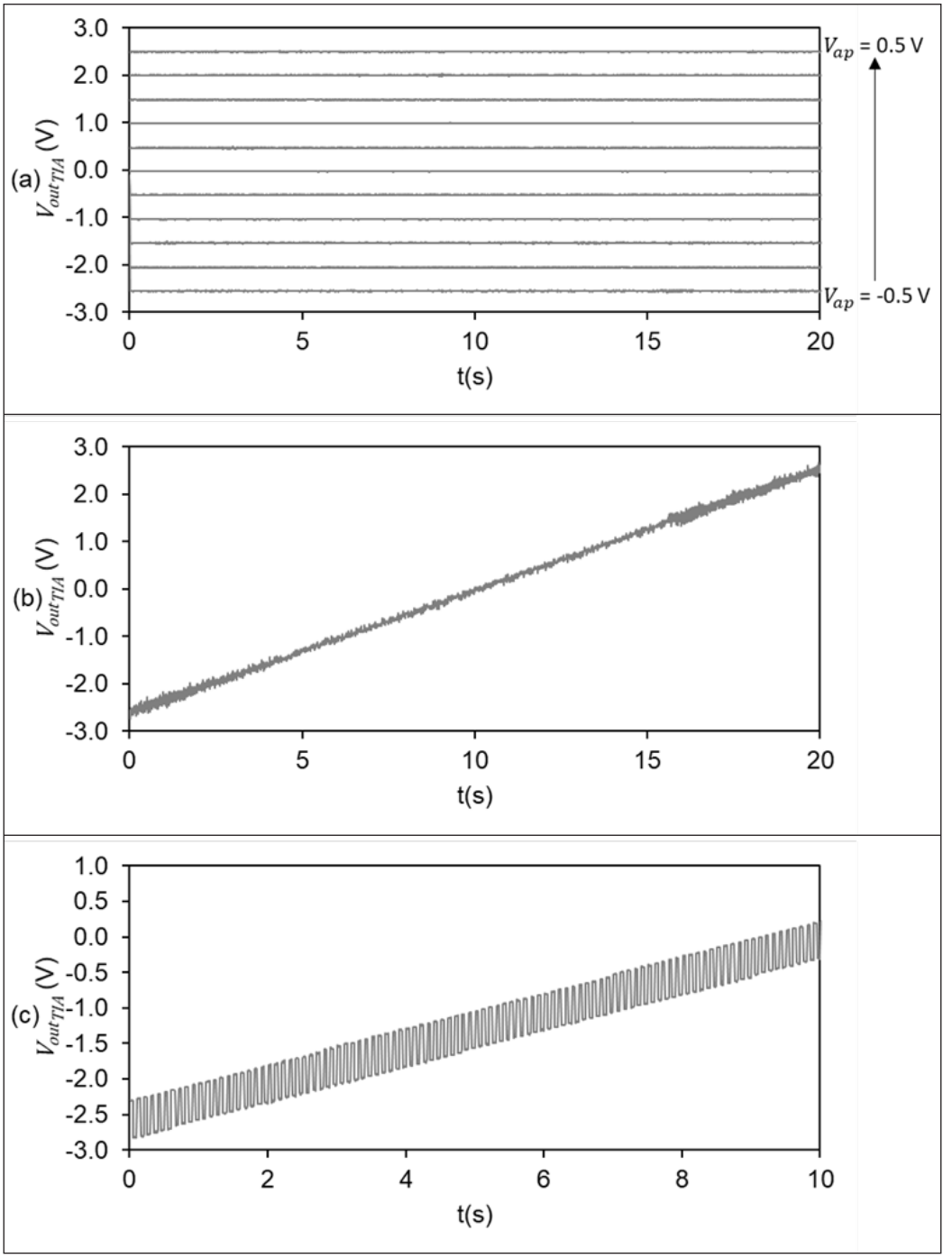

Figure 15. The output of CMP under (a) constant, (b) ramp, and (c) SWV V_{ap} signals, respectively

Accuracy Performance

The accuracy of the HMstat is assessed by plotting the voltammogram shown in Figure 16. The dashed line represents the best-fit line through the data. The R^2 value indicates the correlation coefficient of the best-fit line, where a value of 1 signifies that the data point lies perfectly on the straight line. The equation of the straight line $y = 10.0996x + 0.0901$ can be expressed in the form $y = mx + b$, where m represents the slope of the best-fit line and can be calculated as $1/R_{RE/WE}$. From this equation, $R_{RE/WE}$ is calculated to be 99.014 kΩ. Since the $R_{RE/WE}$ used in this study is 100 kΩ ± 5%, the accuracy of the HMstat is calculated to be 99.014%. This measured value falls within the precision rating of the resistor used, which is 95 kΩ to 105 kΩ.

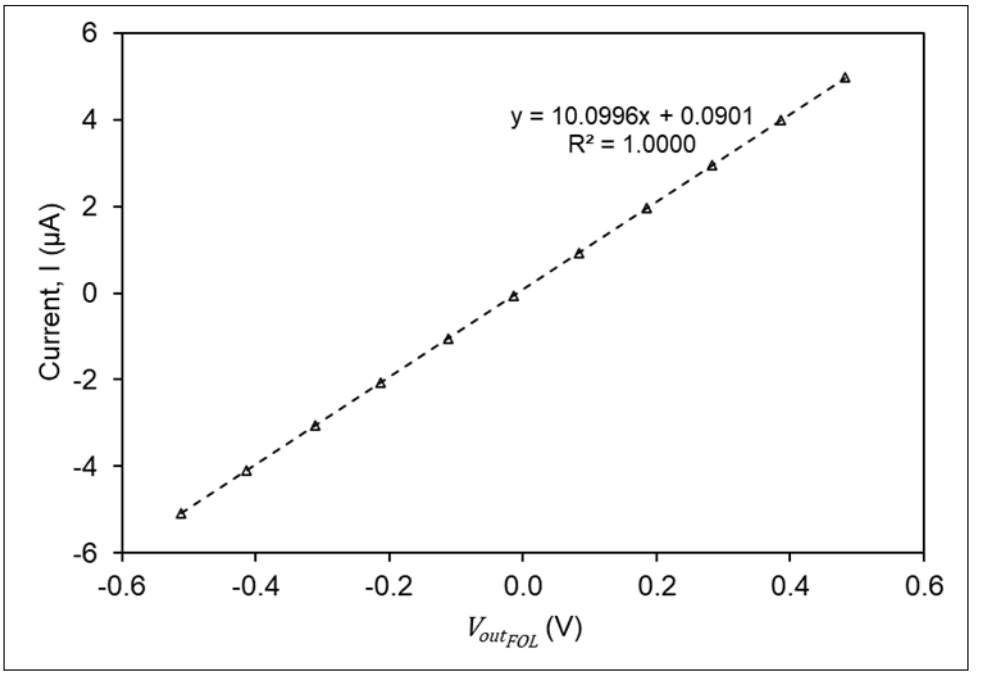

Figure 16. Voltammogram under a variety of constant V_{ap} signal

Comparison to an Existing Solution

The HMstat is compared to an existing solution, which is the Arduino-based potentiostat (Li et al., 2018; Meloni, 2016; Umar et al., 2018). The details of the design and development of the Arduino-based potentiostat are referred to in Umar et al. (2018). For comparison, the parameters of the V_{ap} signals were adapted to those used in the Arduino-based potentiostat. The ramp V_{ap} signal sweeps from an initial potential of -1 V to +1 V with a scan rate of 0.05 V/s. The SWV V_{ap} signal is scanned with an initial potential of -1 V to 0 V, with

modulation and step amplitude of 0.05 V and a frequency of 10 Hz. The R_{gain} and $R_{RE/WE}$ values used in the test were 1 kΩ.

The results are normalized into the current measurement, $1/R_{RE/WE}$ calculated using Equation 3. Figures 17(a) and (b) show the response of HMstat and Arduino-based potentiostat under ramp and SWV V_{ap} signals, respectively. For the ramp V_{ap} signal, both the HMstat and Arduino-based potentiostat exhibit similar increasing patterns in current response, although significant offset and higher noise are observed in the Arduino-based potentiostat's results. The results indicate that both devices can operate under a ramp V_{ap} signal. Existing studies support the result of Arduino-based potentiostat (Cordova-Huaman et al., 2021; Li et al., 2018; Meloni, 2016) that demonstrate its to perform CV and LSV (part of ramp V_{ap} signal).

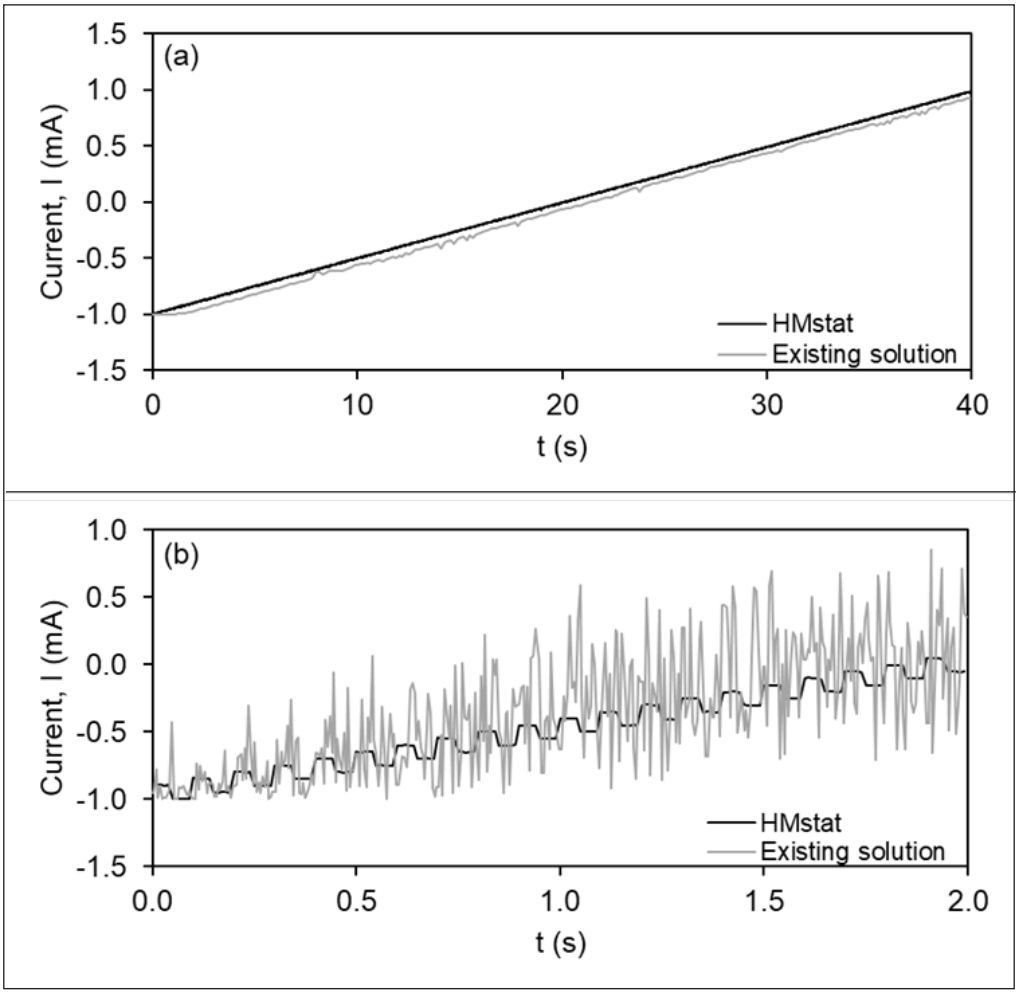

Figure 17. Response of HMstat and the existing solution under the ramp and SWV V_{ap} signal

The results under SWV V_{ap} signals show that the Arduino-based potentiostat produces higher current noise than HMstat [Figure 17(b)]. This is attributed to the Arduino's 8-bit PWM DAC resolution, which is insufficient for performing the SWV V_{ap} signal. In contrast, the HMstat uses a built-in 12-bit DAC resolution, adequate for SWV V_{ap} signals. Consequently, the HMstat demonstrates superior performance in handling SWV V_{ap} signal compared to Arduino-based potentiostat.

CONCLUSION

The design and development of the HMstat have been successfully achieved by employing a two-board potentiostat system. This system comprises the analog component, known as the potentiostat read-out circuit component (PRCC), and the digital component, which is the control signal component (CSC). The implementation of through-hole technology for the PRCC has facilitated the fabrication process, allowing for in-house fabrication and modification, irrespective of the researcher's background. Additionally, the use of the myRIO platform for the CSC has simplified and reduced the stages in the PRCC from the previous design (Umar et al., 2018) to just three stages. This reduction is due to the myRIO platform's built-in 12-bit DAC and ADC, dual polarity analog inputs and outputs, and supply power capabilities. The real-time signals generated and acquired are accessible for monitoring through a GUI developed on the LabVIEW platform.

The capability of HMstat was evaluated through both static and dynamic V_{ap} signals. The HMstat demonstrated its ability to operate under constant, ramp, and SWV V_{ap} signals, indicating its suitability for performing the SWASV method, as the V_{ap} signals are essential components of SWASV. The accuracy of the HMstat was found to be 99.014%, which is within the tolerance range of the components used (5%). Comparative performance verification between HMstat and an existing Arduino-based potentiostat has shown that the HMstat is superior in handling both ramp and SWV V_{ap} signals. The results confirm that the HMstat outperforms the existing solution, demonstrating its enhanced capability and accuracy.

Overall, the specifications of the HMstat are comparable to that of a commercial hand-held potentiostat, as shown in Table 3. The EmStat4S by DropSens comes in two versions: low range and high range. The low range operates within a potential range of ±3 V and a maximum measurable current of ±30 mA. In contrast, the high range operates within ±6 V and a maximum measurable current of ±200 mA. It is capable of performing various voltammetric, amperometric, galvanostatic, and pulse techniques. The DropStat by Metrohm offers a narrower potential range of ±2 V and a maximum measurable current of ±0.2 mA, and it supports some amperometric and voltammetric techniques. Meanwhile, the DropStat Plus provides a wider potential range of ±4V and a maximum measurable current of ± 40 mA, and it is capable of operating amperometric, galvanostatic

and voltammetric techniques. The HMstat offers the widest potential range up to ±10 V. Although its maximum current range is limited to ±0.1 mA, this limit can be adjusted by modifying the feedback gain, R_{gain}, depending on the application. The HMstat is capable of performing techniques used for heavy metal detection, including CV, SWV, and SWASV.

Table 3
Specification of potentiostat

Name	Potential range	Maximum measurable current	Available technique	Device page on the company's website
EmStat4S	±3 V or ±6 V	±30 mA or ±200 mA	Voltammetric: LSV, CV; Amperometric: CA, ZRA, CC, MA, PAD; Galvanostatic: LSP, CP, MP, OCP; Pulsed technique: DPV, SWV, NPV	https://www.palmsens.com/product/emstat4s/?utm_source=google_ads&utm_medium=cpc&utm_campaign=landen&gad_source=1&gclid=CjwKCAiApY-7BhBjEiwAQMrrEROngQ-vwLg-0rgdg0tTt193PyKo3HvoDaphBCcuoWxAtfLTjGpk6hoCLJ0QAvD_BwE
DropStat	± 2V	± 0.2 mA	Amperometric: AD; Voltammetric: LSV, CV, SWV, DPV	https://metrohm-dropsens.com/products/instruments/electrochemical-instruments/electrochemical-reader-dropstat/
DropStat Plus	± 4V	± 40 mA	Amperometric: AD; Voltammetric: LSV, CV, SWV, DPV; Galvanostatic: OCP	https://metrohm-dropsens.com/products/instruments/electrochemical-instruments/standalone-electrochemical-reader-customized-for-your-final-application/
HMstat	±10 V	±0.1 mA	CV, and SWV, and SWASV	-

Chronoamperometric (CA), Zero Resistance Amperometry (ZRA), Chronocoulometry (CC), MultiStep Amperometry (MA), Pulsed Amperometric Detection (PAD), Linear Sweep Potentiometry (LSP), Chronopotentiometry (CP), MultiStep Potentiometry (MP), Open Circuit Potentiometry (OCP), Differential Pulse Voltammetry (DPV), Normal Pulse Voltammetry (NPV)

For further progress, the HMstat should be assessed for detecting heavy metal ions in solution by coupling it with an electrode sensor. To enable in-situ detection, a compact electrode sensor is preferred to meet the intended purpose. A screen-printed electrode sensor is a suitable choice, as it integrates three essential electrodes on the same surface. The pictorial representation of the HMstat coupled with the screen-printed electrode is shown in Figure 18. A small sample solution containing heavy metal ions will be dropped onto the surface of the electrode sensor.

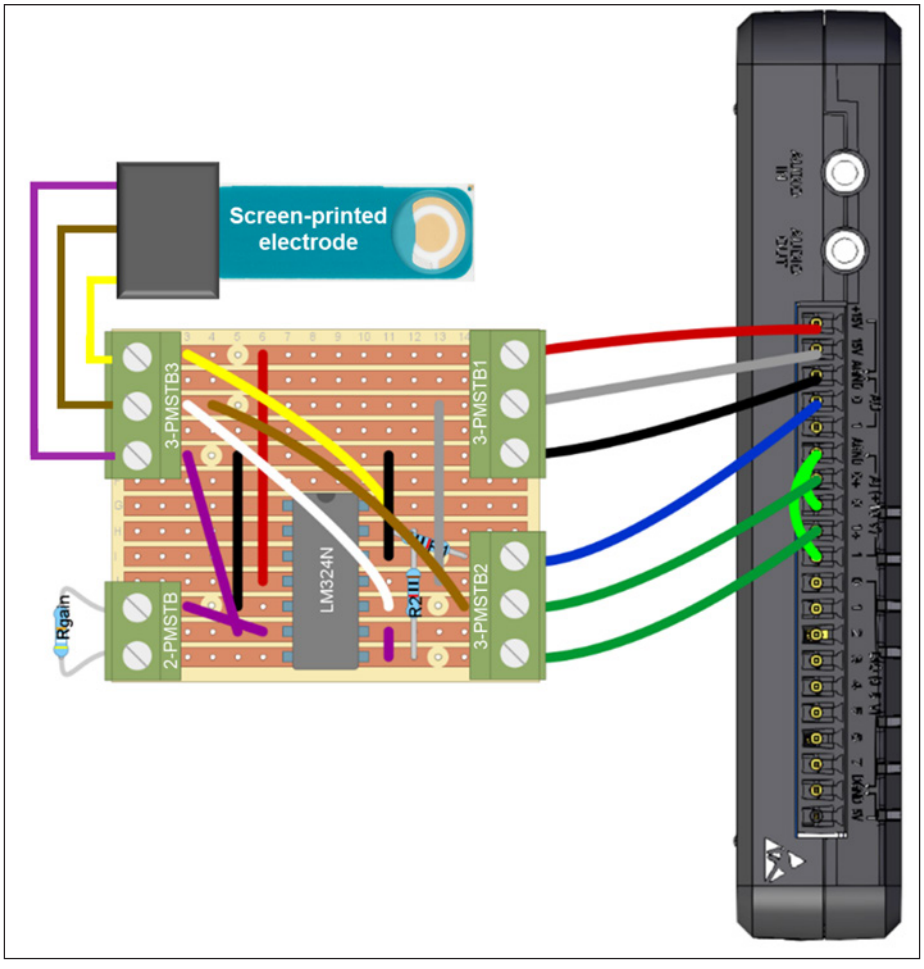

Figure 18. Setup for heavy metal detection using HMstat and screen-printed electrode

ACKNOWLEDGEMENT

Special thanks to Universiti Sains Malaysia for financial assistance through Short Term Grant (R501-LR-RND002-0000000556-0000).

REFERENCES

Adams, S., Doeven, E. H., Quayle, K., & Kouzani, A. (2019). MiniStat: Development and evaluation of a mini-potentiostat for electrochemical measurements. *IEEE Access*, *7*, 31903–31912. https://doi.org/10.1109/ACCESS.2019.2902575

Ahmed, M. F., Mokhtar, M., Alam, L., Mohamed, C. A. R., & Ta, G. C. (2020). Investigating the status of cadmium, chromium and lead in the drinking water supply chain to ensure drinking water quality in Malaysia. *Water*, *12*(10), 1–26. https://doi.org/10.3390/w12102653

Azid, A., Noor, S., Amin, S. M., Khalit, S. I., Ismail, S., Samsudin, M. S., Yusof, K. M. K. K., Latiffah, N., Rani, A., Amran, M. A., Yunus, K., Shakir, A., & Saudi, M. (2018). Determination of selected heavy metals in airborne particles in industrial area: A baseline study. *Malaysian Journal of Fundamental and Applied Sciences*, *14*(2), 251–256.

Bansod, B. K., Kumar, T., Thakur, R., Rana, S., & Singh, I. (2017). A review on various electrochemical techniques for heavy metal ions detection with different sensing platforms. *Biosensors and Bioelectronics*, *94*, 443–455. https://doi.org/10.1016/j.bios.2017.03.031

Bernalte, E., Arévalo, S., Pérez-Taborda, J., Wenk, J., Estrela, P., Avila, A., & Di Lorenzo, M. (2020). Rapid and on-site simultaneous electrochemical detection of copper, lead and mercury in the Amazon river. *Sensors and Actuators, B: Chemical*, *307*, Article 127620. https://doi.org/10.1016/j.snb.2019.127620

Borrill, A. J., Reily, N. E., & Macpherson, J. V. (2019). Addressing the practicalities of anodic stripping voltammetry for heavy metal detection: A tutorial review. *Analyst*, *144*(23), 6834–6849. https://doi.org/10.1039/c9an01437c

Chaudhary, S., Sagar, S., Lal, M., Tomar, A., Kumar, V., & Kumar, M. (2020). Partitioning of heavy metals in different environmental and biotic components in the coastal waters of the Straits of Malacca, Peninsular Malaysia. *Journal of Environment Biology*, *41*, 812–820.

Cordova-Huaman, A. V., Jauja-Ccana, V. R., & La Rosa-Toro, A. (2021). Low-cost smartphone-controlled potentiostat based on Arduino for teaching electrochemistry fundamentals and applications. *Heliyon*, *7*(2), Article e06259. https://doi.org/10.1016/j.heliyon.2021.e06259

Dryden, M. D. M. M., & Wheeler, A. R. (2015). DStat: A versatile, open-source potentiostat for electroanalysis and integration. *PLOS ONE*, *10*(10), 1–17. https://doi.org/10.1371/journal.pone.0140349

Fakude, C. T., Arotiba, O. A., & Mabuba, N. (2020). Electrochemical aptasensing of cadmium (II) on a carbon black-gold nano-platform. *Journal of Electroanalytical Chemistry*, *858*, Article 113796. https://doi.org/10.1016/j.jelechem.2019.113796

IARC. (2012). Cadmium and cadmium compounds. In *Arsenic, Metals, Fibres and Dusts* (pp. 121–145). International Agency for Research on Cancer.

Irving, P., Cecil, R., & Yates, M. Z. (2021). MYSTAT: A compact potentiostat/galvanostat for general electrochemistry measurements. *HardwareX*, *9*, Article e00163. https://doi.org/10.1016/j.ohx.2020.e00163

Ishak, A. R., Zuhdi, M. S. M., & Aziz, M. Y. (2020). Determination of lead and cadmium in tilapia fish (*Oreochromis niloticus*) from selected areas in Kuala Lumpur. *The Egyptian Journal of Aquatic Research*, *46*(3), 221–225. https://doi.org/10.1016/j.ejar.2020.06.001

Janaydeh, M., Ismail, A., Zulkifli, S. Z., & Omar, H. (2019). Toxic heavy metal (Pb and Cd) content in tobacco cigarette brands in Selangor state, Peninsular Malaysia. *Environmental Monitoring and Assessment*, *191*, Article 8. https://doi.org/10.1007/s10661-019-7755-y

Kusin, F. M., Azani, N. N. M., Syed Hasan, S. N. M., & Sulong, N. A. (2018). Distribution of heavy metals and metalloid in surface sediments of heavily-mined area for bauxite ore in Pengerang, Malaysia and associated risk assessment. *Catena*, *165*, 454–464. https://doi.org/10.1016/j.catena.2018.02.029

Li, Y. C., Melenbrink, E. L., Cordonier, G. J., Boggs, C., Khan, A., Isaac, M. K., Nkhonjera, L. K., Bahati, D., Billinge, S. J., Haile, S. M., Kreuter, R. A., Crable, R. M., & Mallouk, T. E. (2018). An easily fabricated low-cost potentiostat coupled with user-friendly software for introducing students to electrochemical reactions and electroanalytical techniques [Product-review]. *Journal of Chemical Education*, *95*(9), 1658–1661. https://doi.org/10.1021/acs.jchemed.8b00340

Lu, Y., Liang, X., Niyungeko, C., Zhou, J., Xu, J., & Tian, G. (2018). A review of the identification and detection of heavy metal ions in the environment by voltammetry. *Talanta*, *178*(2018), 324–338. https://doi.org/10.1016/j.talanta.2017.08.033

Lv, Z. L., Qi, G. M., Jiang, T. J., Guo, Z., Yu, D. Y., Liu, J. H., & Huang, X. J. (2017). A simplified electrochemical instrument equipped with automated flow-injection system and network communication technology for remote online monitoring of heavy metal ions. *Journal of Electroanalytical Chemistry*, *791*(2017), 49–55. https://doi.org/10.1016/j.jelechem.2017.03.012

Meloni, G. N. (2016). Building a microcontroller based potentiostat: A inexpensive and versatile platform for teaching electrochemistry and instrumentation. *Journal of Chemical Education*, *93*(7), 1320–1322. https://doi.org/10.1021/acs.jchemed.5b00961

Mohamed, R. M. S. R., Aziz, F. H. C., & Kassim, A. H. M. (2014). An assessment of selected heavy metal concentrations (Pb, Cu, Cr, Cd, Ni, Zn) in university campus located in industrial area. *ARPN Journal of Engineering and Applied Sciences*, *9*(12), 2724–2730.

Nemiroski, A., Christodouleas, D. C., Hennek, J. W., Kumar, A. A., Maxwell, E. J., Fernandez-Abedul, M. T., Whitesides, G. M., & Paper, S. I. of K. (2014). Universal mobile electrochemical detector designed for use in resource-limited applications. *Proceedings of the National Academy of Sciences*, *111*(33), 11984–11989. https://doi.org/10.1073/pnas.1405679111

Poong, J. H., Tee, L. S., Tan, E., Yip, T. H., Ramli, M. H., Hassan, A. R. A., Ali, A., Meng-Hsien, C., Wah, J. L. C., & Chuan, O. M. (2020). Level of heavy metals in bamboo sharks (*Chiloscyllium* sp.) in Straits of Malacca, Malaysia. *Malaysian Journal of Analytical Sciences*, *24*(4), 546–557.

Rowe, A. A., Bonham, A. J., White, R. J., Zimmer, M. P., Yadgar, R. J., Hobza, T. M., Honea, J. W., Ben-Yaacov, I., & Plaxco, K. W. (2011). CheapStat: An open-source, "do-it-yourself" potentiostat for analytical and educational applications. *PLoS ONE*, *6*(9), Article e23783. https://doi.org/10.1371/journal.pone.0023783

Tichter, T., Gernhard, M., & Vesborg, P. C. K. (2023). PolArStat: An Arduino based potentiostat for low-power electrochemical applications. *Electrochimica Acta*, *469*, Article 143119. https://doi.org/10.1016/j.electacta.2023.143119

Umar, S. N. H., Bakar, E. A., Kamaruddin, N. M., & Uchiyama, N. (2020). A prototype development and evaluation of electrochemical device for heavy metal measurement. In *Proceedings of International Conference of Aerospace and Mechanical Engineering 2019* (pp. 117-125). Springer. https://doi.org/10.1007/978-981-15-4756-0_11

Umar, S. N. H., Akhtar, M. N., Bakar, E. A., Kamaruddin, N. M., & Othman, A. R. (2020). Development of heavy metal potentiostat for batik industry. *Applied Sciences*, *10*(21), Article 7804. https://doi.org/10.3390/app10217804

Umar, S. N. H., Bakar, E. A., Kamaruddin, N. M., & Uchiyama, N. (2018). A low cost potentiostat device for monitoring aqueous solution. *MATEC Web of Conferences*, *217*(04001), Article 8. https://doi.org/10.1051/matecconf/201821704001

Umar, S. N. H., Bakar, E. A., Kamaruddin, N. M., Uchiyama, N., & Akhtar, M. N. (2021). Performance of heavy metal potentiostat for batik industry. In *Intelligent Manufacturing and Mechatronics: Proceedings of SympoSIMM 2020* (pp. 885-894). Springer. https://doi.org/10.1007/978-981-16-0866-7_77

Vanar, M. (2021, October 12). Cadmium found in elephant carcasses. *The Star Online*. https://www.thestar.com.my/news/nation/2021/10/12/cadmium-found-in-elephant-carcasses

Wu, P., Vazquez, G., Mikstas, N., Krishnan, S., & Kim, U. (2017). Aquasift: A low-cost, hand-held potentiostat for point-of-use electrochemical detection of contaminants in drinking water. In *2017 IEEE Global Humanitarian Technology Conference (GHTC)* (pp. 1-4). IEEE Publishing. https://doi.org/10.1109/GHTC.2017.8239306

Zanuri, N. B. M., Abdullah, M. B., Darif, N. A. M., Nilamani, N., & Hwai, A. T. S. (2020). Case study of marine pollution in Teluk Bahang, Penang, Malaysia. In *IOP Conference Series: Earth and Environmental Science* (Vol. 414, No. 1, p. 012032). IOP Publishing. https://doi.org/10.1088/1755-1315/414/1/012032

Zulkifli, H. M., Elias, S. M., Aris, A. Z., Bakar, S. A., & Noor, F. A. M. (2019). Seafood consumption and blood cadmium level of respondents along the coastal area of Melaka, Malaysia. *Malaysian Journal of Medicine and Health Sciences*, *15*(SP4), 68–75.